Journal of Catalysis 272 (2010) 235–245

Contents lists available at ScienceDirect

Journal of Catalysis

journal homepage: www.elsevier.com/locate/jcat

Effects of sulfur on Mo_2C and Pt/Mo_2C catalysts: Water gas shift reaction

Joshua A. Schaidle, Adam C. Lausche, Levi T. Thompson *

University of Michigan, Department of Chemical Engineering, 3020 H.H. Dow Building, 2300 Hayward Street, Ann Arbor, MI 48109-2136, USA

ARTICLE INFO

Article history:
Received 26 January 2010
Revised 7 April 2010
Accepted 8 April 2010
Available online 21 May 2010

Keywords:
Molybdenum carbide
Water gas shift
Sulfur poisoning
H_2S
Platinum

ABSTRACT

Molybdenum carbide (Mo_2C) and Pt/Mo_2C catalysts were evaluated for the water gas shift reaction without and with 5 ppm H_2S. The Mo_2C catalyst was quickly poisoned by sulfur, achieving a rate that was ~10% of that prior to sulfur exposure. The Pt/Mo_2C catalyst was initially more active than the Mo_2C catalyst and deactivated more gradually to a level similar to that for the Mo_2C catalyst. X-ray photoelectron spectroscopy revealed Mo_2C, MoS_2, and S–Mo on the spent catalysts; the Pt/Mo_2C catalyst also contained PtS. The results are consistent with Mo_2C sites on the Mo_2C and Pt/Mo_2C catalysts being partially sulfur tolerant, in that these sites could be reactivated on treatment in 15% CH_4/H_2 at 590 °C. High activity sites associated with Pt nanoparticles were irreversibly deactivated. Residual activities for the Mo_2C and Pt/Mo_2C catalysts in the presence of H_2S appeared to be associated primarily with the presence of MoS_2 domains.

1. Introduction

Sulfur is a contaminant in fossil fuels including crude oil and coal, and often remains in products derived from fossil fuels. Sulfur can also be present in biomass-derived products. For example, Robinson et al. [1] reported that, depending on the type of biomass, the sulfur content varied from ~14–2200 ppm. Sulfur severely and irreversibly deactivates most catalytic materials, and typically has to be removed upstream of the reactor. For some reactions, early transition metal carbides and nitrides have been reported to be sulfur tolerant, in particular at high temperatures and/or pressures [2–4]. For example, DaCosta et al. [3] report that tetralin hydrogenation activities for Mo_2C/Al_2O_3 and WC/Al_2O_3 catalysts were not significantly impacted by the presence of 200 ppm H_2S at 300 °C and 4 MPa. Carbides and nitrides can be synthesized with high surface areas (up to 200 m^2/g) and are catalytically active for a variety of reactions including hydrodesulfurization [4], alcohol amination [5], alkane isomerization [6], alkane hydrogenolysis [7], and CO hydrogenation [8]. Because of their high surface areas, carbides and nitrides have attracted attention for use as support materials, especially for electrocatalysts where their high electronic conductivities can be exploited [9–11]. Recently, a technique has been developed to support metals like Pt and Ni directly onto carbide and nitride surfaces [12]. Some of the resulting materials have been demonstrated to be more active than conventional catalysts for reactions such as water gas shift (WGS) [13] and methanol steam reforming [14].

Research described in this paper investigated the tolerance of Mo_2C and Pt/Mo_2C catalysts to sulfur exposure during the WGS reaction

$$CO + H_2O \leftrightarrow CO_2 + H_2 \quad \Delta H^\circ = -41.1 \text{ kJ/mol} \tag{1}$$

This reaction is a critical step in the conversion of hydrocarbon and alcohol feedstocks into reformate or syngas [15]. Due to the intolerance of most WGS catalysts, sulfur concentrations in the feed typically have to be reduced to ppb levels [16]. The effects of H_2S exposure on the WGS activities of Mo_2C and Pt/Mo_2C catalysts were evaluated, and the materials were characterized to define any associated changes in catalyst structure and composition. Hydrogen sulfide was used as the sulfur species because it is often present in process streams [17]. Results presented in this paper were determined at more moderate temperatures and pressures than those used in most prior investigations [2–4] and provide new insights into the effects of sulfur on the catalytic properties of Mo_2C-based catalysts.

2. Materials and methods

2.1. Catalyst preparation

The Mo_2C catalyst was synthesized using a temperature-programmed reaction procedure [18]. Approximately 1.3 g of ammonium paramolybdate (AM, $(NH_4)_6Mo_7O_{24}{\cdot}4H_2O$, 81–83% MoO_3, Alpha-Aesar) was loaded into a quartz tube reactor on top of a quartz wool plug. In order to maintain consistent catalyst properties, the AM was sieved to 125–250 μm prior to carburization. The AM was reduced in H_2 at 375 mL/min as the

* Corresponding author. Fax: +1 734 763 0459.
E-mail address: ltt@umich.edu (L.T. Thompson).

0021-9517/$ - see front matter © 2010 Elsevier Inc. All rights reserved.
doi:10.1016/j.jcat.2010.04.004

temperature was increased from room temperature (RT) to 350 °C (heating rate of 278 °C/h), and then held at this temperature for 12 h. The reactant gas was then switched from H_2 to a 15% CH_4/H_2 mixture and the temperature was increased from 350 °C to 590 °C at a rate of 160 °C/h. The final temperature was maintained for 2 h prior to quenching the material to RT. This procedure has been shown to produce β-Mo_2C [19]. The resulting material was passivated using a 1% O_2/He mixture at 20 mL/min for at least 5 h.

The Mo_2C-supported Pt catalyst was prepared via wet impregnation of the unpassivated Mo_2C with a deaerated aqueous solution containing 1.3 mg/mL of dihydrogen hexachloriplatinate hexahydrate ($H_2PtCl_6{\cdot}6H_2O$, 99.95% metal basis, Alfa Aesar). After decanting the excess solution, the material was loaded into a quartz reactor and dried in H_2 at 375 mL/min for 3 h at RT. Subsequently, the temperature was increased to 110 °C in ~1 h and held there for 2 h. The temperature was then increased to 450 °C at a rate of 340 °C/h and held for 4 h. Finally, the material was quenched to room temperature and passivated in a 1% O_2/He mixture at 20 mL/min for at least 5 h.

2.2. Characterization

X-ray diffraction analysis was performed using a Rigaku Miniflex Diffractometer with Cu Kα radiation and a Ni filter (λ = 1.540 Å). The range ($10° < 2\theta < 90°$) was scanned at a rate of 5°/min with a 0.02° step size. The BET surface areas were determined via N_2 physisorption using a Micromeritics ASAP 2010 analyzer. Prior to these measurements, the catalysts were degassed at 300 °C for 4 h. Pulse chemisorption experiments were performed using a Micromeritics AutoChem 2910 Chemisorption Analyzer equipped with a thermal conductivity detector and a mass spectrometer. Prior to analysis, the Mo_2C and Pt/Mo_2C catalysts were pretreated in 15% CH_4/H_2 for 4 h at 590 °C [13]. The catalysts were then degassed in He for 1 h. After cooling to RT, the catalysts were repeatedly dosed with 5 mL of 5% CO/He until saturation was achieved. The $Cu/Zn/Al_2O_3$ catalyst was reduced in 5% H_2/Ar at 200 °C until complete reduction of Cu was achieved. The sample was then degassed in flowing He for 1 h and cooled to 60 °C. The gas flow was then switched to N_2O for 1.5 h. The N_2O flow was then replaced with He, and the sample was cooled to RT. The N_2O uptake was determined by performing a H_2 temperature-programmed reduction and measuring the H_2 consumption.

The catalyst compositions were determined by inductively coupled plasma optical emission spectroscopy (ICP–OES) using a Varian 720-ES analyzer. The materials were dissolved in aqua regia (3 parts HCl–1 part HNO_3) and the emission spectra of dissolved species were compared to those for a series of standard solutions of known concentrations. The surface morphologies of the fresh and spent catalysts were characterized using scanning electron microscopy (SEM) with a Phillips XL30 FEG SEM operating at an accelerating voltage of 15–25 kV and a nominal resolution of 2–5 nm. Prior to analysis, the materials were sputter coated with Pd–Au to mitigate charging effects. Sulfur adsorption/incorporation experiments were performed using the microbalance on a TA Instruments Q50 Thermogravimetric Analyzer. These experiments characterized interactions of the catalyst with H_2S. The flow rate to catalyst ratio and temperatures were similar to those used during the reaction rate measurements.

The fresh and spent catalysts were characterized using X-ray photoelectron spectroscopy (XPS) to determine the compositions and oxidation states of species on the surfaces. The XPS experiments were performed using a Kratos Axis Ultra X-ray photoelectron spectrometer with an Al anode (K_α radiation at 1486.6 eV) operating at 10 mA and 14 kV. The spectrometer was equipped with an *in situ* XPS reaction chamber. The spectra were deconvoluted using a nonlinear least squares method employing a combination of Gaussian (80%) and Lorentzian (20%) distributions and CasaXPS, a commercially available XPS analysis program. Parameter constraints were imposed during deconvolution of the Mo, Pt, and S spectra. The Mo 3d spectra were fit using doublets with a splitting of 3.2 eV between the $3d_{5/2}$ and $3d_{3/2}$ peaks and an intensity ratio of 3:2. The Pt 4f spectra were fit using doublets with a splitting of 3.3 eV between the $4f_{7/2}$ and $4f_{5/2}$ peaks and an intensity ratio of 4:3. The S 2p spectra were fit using doublets with a splitting of 1.2 eV between the $2p_{3/2}$ and $2p_{1/2}$ peaks and an intensity ratio of 2:1. For all spectra, the peak widths (FWHM) for the doublets were constrained to be similar. Shirley backgrounds were used for the Mo 3d, Pt 4f, and S 2p spectra, while a linear background was used for the C 1s and O 1s spectra. The peak areas were normalized using the appropriate atomic sensitivity factors. This allowed comparison of the relative atomic fractions of each species on the catalyst surfaces.

2.3. Reaction rate measurements

The WGS rates were measured using a 4 mm I.D. quartz U-tube in which 20–30 mg of catalyst was supported on a quartz wool plug. As necessary, the catalysts were diluted with inert, low surface area (<1 m^2/g) silica to prevent channeling, avoid problems with axial dispersion, and minimize temperature gradients in the bed. Prior to the reaction rate measurements, the catalysts were pretreated at 590 °C for 4 h in a mixture of 15% CH_4/H_2 [13]. The effluent gas was passed through an ice-bathed condenser to remove most of the H_2O, and the composition was analyzed using a SRI 8610C gas chromatograph (GC) equipped with a Supelco Carboxen-1000 column and a thermal conductivity detector. The GC sampled the effluent gas every 30 min. To ensure that there was no residual sulfur, the reactor system (reactor and lines) was heated to 500 °C in flowing H_2 for 12 h in between runs. This treatment was sufficient to reproduce the sulfur-free WGS rate for a commercial Cu–Zn–Al benchmark catalyst.

The rates were measured under differential conditions (conversion $\leqslant$10%) at atmospheric pressure over a temperature range of 200–240 °C. The equilibrium WGS conversion under conditions used in the experiments would be greater than 90%. The dry reactant simulated the effluent stream from a partial oxidation reformer and consisted of 13% CO, 56% H_2, 8% CO_2, and balance N_2. The dry reactant was passed through a H_2O saturator maintained at 69.4 ± 0.4 °C resulting in a wet reactant containing 30% H_2O. The flow rate of the reactant was 262 mL/min corresponding to a gas hourly space velocity of 125,000 h^{-1}. Hydrogen production (CO consumption) rates and conversions were determined by monitoring the concentration of CO in the product stream. Features attributable to H_2 were present in the chromatograms but could not be quantified because He was used as the carrier gas. No products other than CO_2 and H_2 were observed in the effluent.

For measurements including sulfur, the catalysts were initially allowed to achieve pseudo steady-state rates at 240 °C in the sulfur-free reactant stream. Subsequently, H_2S was added to the reactant stream to produce concentrations ranging up to 50 ppmv. In order to maintain the same gas hourly space velocity, the N_2 balance gas flow rate was adjusted to account for the addition of H_2S. The regenerability of the catalysts was investigated by treating the spent materials in 15% CH_4/H_2 for 4 h at 590 °C. After this treatment, the catalysts were again exposed to the sulfur-free feed at 240 °C to determine the recovered rate.

3. Results

3.1. Pre-reaction characterization

Diffraction patterns for the Mo_2C and Pt/Mo_2C catalysts (Fig. 1) contained peaks for β-Mo_2C [20] and α-MoC_{1-x} [21]. The relative peak areas suggested similar amounts of each. These phases have Mo:C ratios near two; therefore, we will refer to this material as Mo_2C. No peaks were observed for MoO_2 [22] or MoO_3 [23], indicating that synthesis achieved complete bulk carburization. There were no clearly discernable Pt peaks for the Pt/Mo_2C catalyst [24], indicating that crystallites, if present, were below the detection limit of the X-ray diffractometer. A detailed description of the Pt dispersion is beyond the scope of this work, but will be explored in a subsequent paper. Results from catalyst characterization are given in Table 1. The reduced surface area for the Pt/Mo_2C catalyst compared to the Mo_2C catalyst may be due to pore blocking by Pt nanoparticles. Interestingly, the addition of Pt decreased the CO uptake when compared to Mo_2C.

The *in situ* XPS results tracked effects of the various treatments on the catalyst surface chemistries without exposure to air. Following treatment, the samples were purged with N_2 then cooled to room temperature in the *in situ* XPS reaction chamber. The pressure was reduced to $<10^{-8}$ Torr, and the samples were transferred into the analysis chamber. Results from the deconvolution of spectra for the as-synthesized and pretreated (15% CH_4/H_2 at 590 °C for

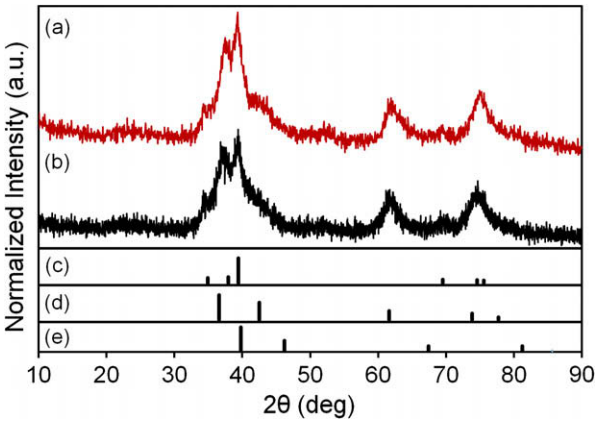

Fig. 1. X-ray diffraction patterns for the (a) Pt/Mo_2C and (b) Mo_2C catalysts, and peak positions for polycrystalline (c) β-Mo_2C [20], (d) α-MoC_{1-x} [21], and (e) Pt [24] reference materials.

Table 1
BET surface areas, N_2O uptakes, CO uptakes, site densities, Pt loadings, and TOFs for Mo_2C, Pt/Mo_2C, $Cu/Zn/Al_2O_3$, and Pt/oxide catalysts.

Catalyst	BET surface area (m^2/g)	N_2O uptake (μmol/g)	CO uptake (μmol/g)	Site density[a] (sites/$m^2 \times 10^{18}$)	Pt loading (wt.%)	TOF (s^{-1})
Mo_2C	98	–	268	1.65	–	0.08[c]
Pt/Mo_2C	70	–	151	1.30	3.7[b]	0.80[c]
$Cu/Zn/Al_2O_3$	60	192	–	1.93	–	0.32[c]
Pt/Al_2O_3 [25]	180	–	91	0.31	3	0.03[d]
Pt/ZrO_2 [25]	75	–	56	0.45	3	0.20[d]
Pt/TiO_2 [25]	74	–	9	0.07	3	0.82[d]

[a] Determined from uptake and BET surface area.
[b] Determined using ICP–OES. Corresponds to a surface coverage of 12%, assuming 10 Pt atoms/nm^2.
[c] Based on rates measured at 240 °C. Extrapolated TOFs for the Mo_2C, Pt/Mo_2C, and $Cu/Zn/Al_2O_3$ catalysts at 250 °C are 0.11 s^{-1}, 1.02 s^{-1}, and 0.44 s^{-1}, respectively.
[d] Based on rates measured at 250 °C.

Table 2
Binding energies for species on the surfaces of the as-synthesized and pretreated Mo_2C and Pt/Mo_2C catalysts.

Catalyst	Treatment	C 1s (eV)[a,b]			Mo $3d_{5/2}$ (eV)[a]				Pt $4f_{7/2}$ (eV)[a]		O 1s (eV)[a]		
		Mo_2C	C–O	C=O	Mo^{2+}	$Mo^{\delta+}$	Mo^{4+}	Mo^{6+}	Pt^0	Pt^{2+}	MoO_x	PtO	O^-, OH^-, H_2O, O=C
Mo_2C		283.5 (22)	286.1 (26)	288.8 (13)	228.5 (15)	229.0 (16)	229.6 (19)	232.4 (50)	–	–	530.8 (64)	–	532.2 (36)
Mo_2C	CH_4/H_2[c]	283.6 (48)	287.3 (2)	–	228.5 (55)	228.8 (23)	229.6 (19)	–	–	–	530.6 (81)	–	532.2 (19)
Pt/Mo_2C		283.5 (6)	286.6 (16)	288.2 (18)	228.5 (23)	228.8 (27)	229.8 (25)	232.3 (25)	71.6 (78)	72.7 (22)	530.6 (37)	531.5 (21)	532.6 (42)
Pt/Mo_2C	CH_4/H_2[c]	283.6 (23)	286.1 (22)	–	228.5 (51)	228.8 (31)	229.9 (14)	–	71.8 (85)	73.3 (15)	530.7 (37)	531.8 (8)	532.4 (55)

[a] The number in parentheses represents the atomic percentage.
[b] Balance of atomic percentages for C 1s is adventitious carbon.
[c] Pretreated in 15% CH_4/H_2 at 590 °C for 4 h, purged with N_2, then cooled to room temperature.

4 h) catalysts are summarized in Table 2. Peaks that accounted for less than 10% of the total spectral area typically did not contribute significantly to the goodness of fit. Surfaces of the catalysts contained varying concentrations of species attributable to Mo_2C, Mo and Pt oxides, and carbon oxides; no chlorine residue (from the Pt precursor) was observed for the Pt/Mo_2C catalyst. The C 1s spectra for the Mo_2C and Pt/Mo_2C catalysts are shown in Fig. 2. Peaks centered at 284.8 eV corresponded to adventitious carbon and were used to reference the other binding energies. In addition to adventitious carbon, surfaces of the Mo_2C and Pt/Mo_2C catalysts contained carbidic carbon and adsorbed carbon oxides. Peaks at 283.5 ± 0.1 eV were assigned to carbidic carbon in Mo_2C [26]. The peaks at 286.6 ± 0.6 eV and 288.4 ± 0.4 eV were assigned to species containing C—O and C═O bonds, respectively [27,28]. These could be associated with carbonates and/or formates on the catalyst surface.

The Mo 3d spectra for the Mo_2C and Pt/Mo_2C catalysts contained four doublets (see Fig. 2). Doublets with Mo $3d_{5/2}$ peaks at 232.3 ± 0.2 eV are characteristic of Mo^{6+} and suggested the presence of MoO_3 [2,27,29,30]. The peaks at 229.7 ± 0.2 eV were likely due to Mo^{4+} in MoO_2 [27,30,31]. The peaks at 228.5 ± 0.1 eV were assigned to Mo^{2+} in Mo_2C, based on comparisons with spectra reported in the literature [2,26,32,33]. For most of the materials, the ratio of the normalized area for the C 1s peak at 283.5 ± 0.1 eV to the normalized area for the Mo $3d_{5/2}$ peak at 228.5 ± 0.1 eV was consistent with the presence of Mo_2C (see Table 3). The Mo $3d_{5/2}$ peak at 228.9 ± 0.1 eV was designated as $Mo^{\delta+}$ ($2 < \delta < 4$), perhaps in an oxycarbide [30,34].

The O 1s spectra for the Mo_2C and Pt/Mo_2C catalysts are also shown in Fig. 2. Two different species were present on the Mo_2C surfaces. Peaks at 530.7 ± 0.2 eV are typically assigned to oxygen in Mo oxides [26,27,29,30]. Peaks at 532.4 ± 0.2 eV are indicative of strongly bound O^-, OH^-, H_2O and/or O═C [28,30]. Spectra for the Pt/Mo_2C catalyst contained an additional peak at 531.7 ± 0.2 eV corresponding to Pt oxide [35,36].

Two doublets were observed in the Pt 4f XPS spectra (Fig. 3). The dominant doublet with Pt $4f_{7/2}$ peak at 71.7 ± 0.1 eV was assigned to Pt^0 [36,37]. The minor component with Pt $4f_{7/2}$ peak at 73.0 ± 0.3 eV was assigned to Pt^{2+}, most likely in the form of PtO [37].

Pretreatment of the as-synthesized catalysts in 15% CH_4/H_2 at 590 °C for 4 h caused a significant change in the surface chemistry. The percentage of Mo in the form of Mo_2C increased from 15 to 20% in the as-synthesized catalysts to more than 50% in the pretreated catalysts. Pretreatment completely reduced the Mo^{6+} concentration and caused the formation of a small amount of a species with Mo $3d_{5/2}$ peaks at 231.0 ± 0.1 eV (see Fig. 2). Peaks with similar binding energies have been assigned to Mo^{5+} [29–31]. Pretreatment also increased the relative amount of carbidic carbon at the surface and decreased the amount of oxygen and carbon oxides

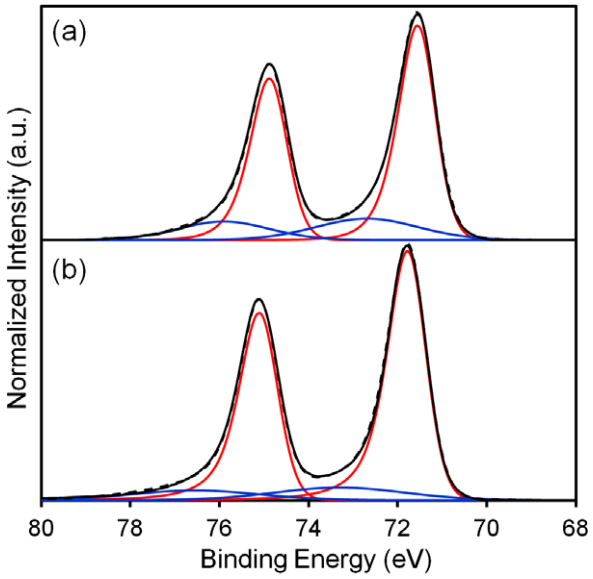

Fig. 3. Pt 4f XPS spectra for the (a) as-synthesized and (b) pretreated Pt/Mo_2C catalyst. The catalyst was pretreated at 590 °C for 4 h in a mixture of 15% CH_4/H_2.

Table 3
Selected atomic ratios for species on surfaces of the as-synthesized and pretreated Mo_2C and Pt/Mo_2C catalysts.

Catalyst	Treatment	C[a]/Mo[b] ratio	O/Mo ratio	O[c]/Pt[d] ratio
Mo_2C		1.9	2.6	–
Mo_2C	CH_4/H_2[e]	0.7	1.5	–
Pt/Mo_2C		0.5	1.9	0.8
Pt/Mo_2C	CH_4/H_2[e]	0.5	1.2	0.4

[a] C 1s peak corresponding to carbidic carbon (283.5 ± 0.1 eV).
[b] Mo 3d doublet corresponding to Mo^{2+} (228.5 ± 0.1 eV).
[c] O 1s peak corresponding to PtO (531.7 ± 0.2 eV).
[d] Pt doublet corresponding to PtO (73.0 ± 0.3 eV).
[e] Pretreated in 15% CH_4/H_2 at 590 °C for 4 h, purged with N_2, then cooled to room temperature.

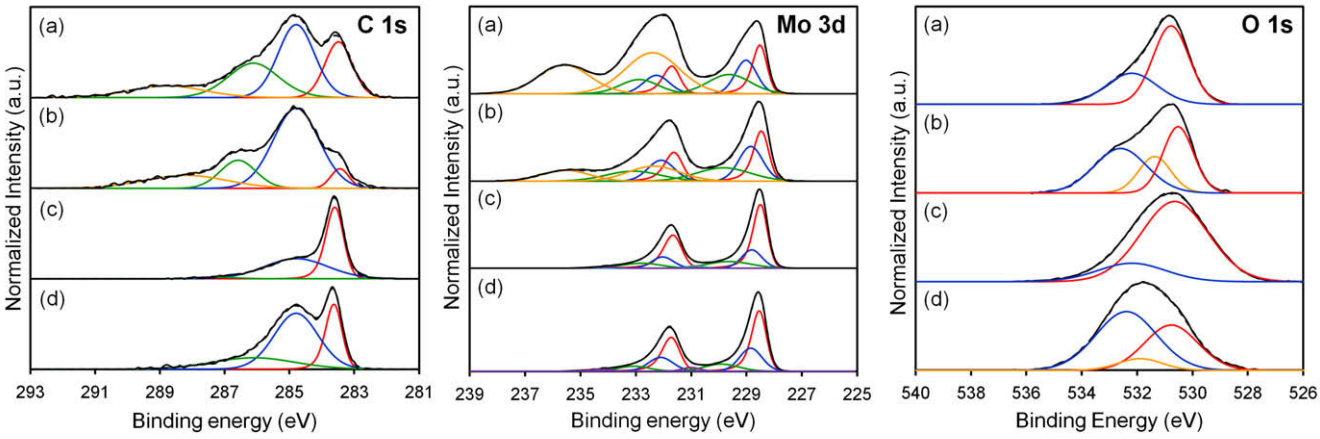

Fig. 2. C 1s, Mo 3d, and O 1s XPS spectra for the (a) as-synthesized Mo_2C catalyst, (b) as-synthesized Pt/Mo_2C catalyst, (c) pretreated Mo_2C catalyst, and (d) pretreated Pt/Mo_2C catalyst. The catalysts were pretreated at 590 °C for 4 h in a mixture of 15% CH_4/H_2.

(Fig. 2). Approximately 70% of Mo on the as-synthesized Mo_2C surface was in the form of MoO_3 and MoO_2, which is in good agreement with an O/Mo ratio of 2.6 (Table 3). The O/Mo ratio for the as-synthesized Pt/Mo_2C catalyst was 1.9. Pretreatment at 590 °C in 15% CH_4/H_2 resulted in a substantial reduction in the O/Mo ratio to 1.5 for Mo_2C and 1.2 for Pt/Mo_2C. While pretreatment reduced the overall oxygen to molybdenum ratio for both catalysts, the presence of Pt on Pt/Mo_2C seemed to facilitate the reduction of Mo oxides to a greater extent than Mo_2C alone. There was only a slight reduction in the percentage of Pt^{2+} after pretreatment with 15% CH_4/H_2 at 590 °C.

3.2. Reaction rates

The WGS rates for the Pt/Mo_2C catalyst were almost an order of magnitude higher than those for the Mo_2C catalyst and 2–3 times higher than those for the $Cu/Zn/Al_2O_3$ catalyst in the absence of H_2S (Fig. 4). The apparent activation energies for the Mo_2C, Pt/Mo_2C, and $Cu/Zn/Al_2O_3$ catalysts were 59, 42, and 47 kJ/mol, respectively. These results are consistent with those reported previously [12,13,18]. Turnover frequencies for the Pt/Mo_2C catalyst determined using CO uptakes were higher than those for the $Cu/Zn/Al_2O_3$ catalyst determined using the N_2O update, and similar to those reported for the most active Pt-based catalysts (see Table 1).

The Mo_2C and Pt/Mo_2C catalysts deactivated during the first 10–15 h of exposure to sulfur-free reformate. Fig. 5 shows the rates for Mo_2C and Pt/Mo_2C at 240 °C as a function of time on stream (TOS). To probe the nature of this deactivation, the activity decay was fit to models of the form [38]:

$$-\frac{da}{dt} = k_d a(t)^m \tag{2}$$

where $a(t)$ is the ratio of the rate at time t to the initial rate, k_d is the specific decay constant, and t is time on stream (TOS). The best-fit for the Mo_2C and Pt/Mo_2C catalysts was obtained using the reciprocal power form (Tables 4 and 5). This form is consistent with deactivation by carbon deposition [39,40].

Rates for the Mo_2C and Pt/Mo_2C catalysts also decreased on exposure to sulfur. After the introduction of 5 ppm H_2S, the hydrogen production rate for the Mo_2C catalyst decreased by ~90% within 10 min. After ~32 h on stream, the catalyst regained some of its activity, reaching a H_2 production rate that was ~25% of its sulfur-free reactant steady-state rate. These temporal trends were reproducible. When H_2S was removed from the reactant, the rate for the Mo_2C catalyst quickly decreased to zero. Upon treating the spent Mo_2C catalyst with 15% CH_4/H_2 at 590 °C for 4 h, 25–30% of its initial rate was recovered.

General temporal trends for the Pt/Mo_2C catalyst were similar to those for the Mo_2C catalyst, although the deactivation rate for the Pt/Mo_2C catalyst was much slower and occurred over a period of several hours. The Pt/Mo_2C catalyst did not regain any of its lost activity after removal of H_2S from the reactant, and treatment in 15% CH_4/H_2 at 590 °C for 4 h resulted in a very slight reactivation of the catalyst to a rate similar to that for the Mo_2C catalyst.

To better understand the nature of interactions between sulfur and the Pt/Mo_2C catalyst, the H_2S concentration in the reactant was varied. The deactivation rates were strong functions of the sulfur concentration. The ratio of the rate following exposure to H_2S to the rate just before exposure to H_2S, $a_s(t)$, is plotted in Fig. 6 as a function of TOS with 5, 25, and 50 ppm H_2S in the reactant. The activity decay was again fit to models of the form [38]:

$$-\frac{da_s}{dt} = k_{d,s} C_{H_2S,0}^{n} a_s(t)^m \tag{3}$$

where $k_{d,s}$ is the specific decay constant due to sulfur exposure, t is the TOS after sulfur introduction, and $C_{H2S,0}$ is the concentration of H_2S in the reactant (assumed to be constant). The best-fit was achieved for $m = 1$ (exponential form) and $n = 0.51 \pm 0.05$, although the hyperbolic form was also a good fit for the data. The fit parameters for each of the models are included in Table 6. The exponential form is typical of deactivation caused by poisoning [41], while the hyperbolic form often indicates deactivation by sintering [38]. The half-order dependence on concentration also suggests that H_2S dissociated on the Pt/Mo_2C catalyst surface [41].

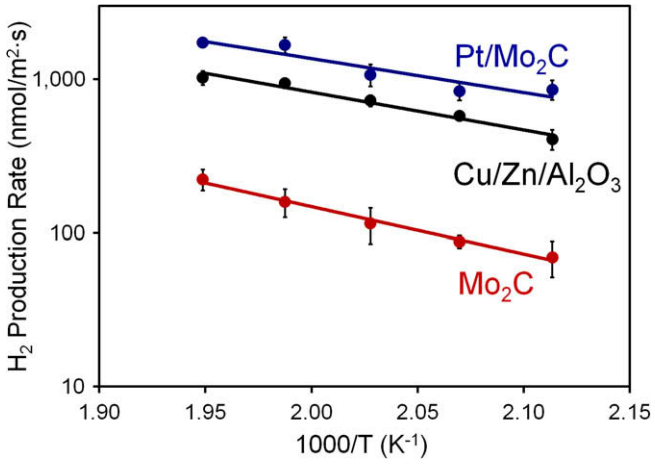

Fig. 4. Hydrogen production rates during WGS for the Mo_2C and Pt/Mo_2C catalysts at 200–240 °C. The H_2 production rates for a commercial $Cu/Zn/Al_2O_3$ catalyst are also illustrated. The reformate feed consisted of 9% CO, 30% H_2O, 6% CO_2, 39% H_2, and 16% N_2.

Table 4
Results from nonlinear regression of sulfur-free activity data for the Mo_2C catalyst to four empirical decay rate laws.

Type	Linear	Exponential	Hyperbolic	Reciprocal power
Differential form	$-\frac{da}{dt} = k_d$	$-\frac{da}{dt} = k_d a$	$-\frac{da}{dt} = k_d a^2$	$-\frac{da}{dt} = k_d A_0^{1/5} a^m$
Integral form	$a = 1 - k_d t$	$a = e^{-k_d t}$	$a = \frac{1}{1+k_d t}$	$a = A_0 t^{-k_d}$
k_d (h^{-1})	0.06 ± 0.01	0.18 ± 0.05	0.41 ± 0.08	0.20 ± 0.02
A_0	–	–	–	0.46 ± 0.03
R^2_{adj}	0.371	0.732	0.893	0.996
F^a	18.3	84.7	260	4140

[a] Calculated by dividing the mean square model by the mean square error. P value for all models was <0.0002.

Table 5
Results from nonlinear regression of sulfur-free activity data for the Pt/Mo_2C catalyst to four empirical decay rate laws.

Type	Linear	Exponential	Hyperbolic	Reciprocal power
Differential form	$-\frac{da}{dt} = k_d$	$-\frac{da}{dt} = k_d a$	$-\frac{da}{dt} = k_d a^2$	$-\frac{da}{dt} = k_d A_0^{1/5} a^m$
Integral form	$a = 1 - k_d t$	$a = e^{-k_d t}$	$a = \frac{1}{1+k_d t}$	$a = A_0 t^{-k_d}$
k_d (h^{-1})	0.045 ± 0.006	0.066 ± 0.009	0.10 ± 0.05	0.136 ± 0.007
A_0	–	–	–	0.75 ± 0.02
R^2_{adj}	0.952	0.970	0.982	0.999
F^a	573	926	1570	60,300

[a] Calculated by dividing the mean square model by the mean square error. P value for all models was <0.0001.

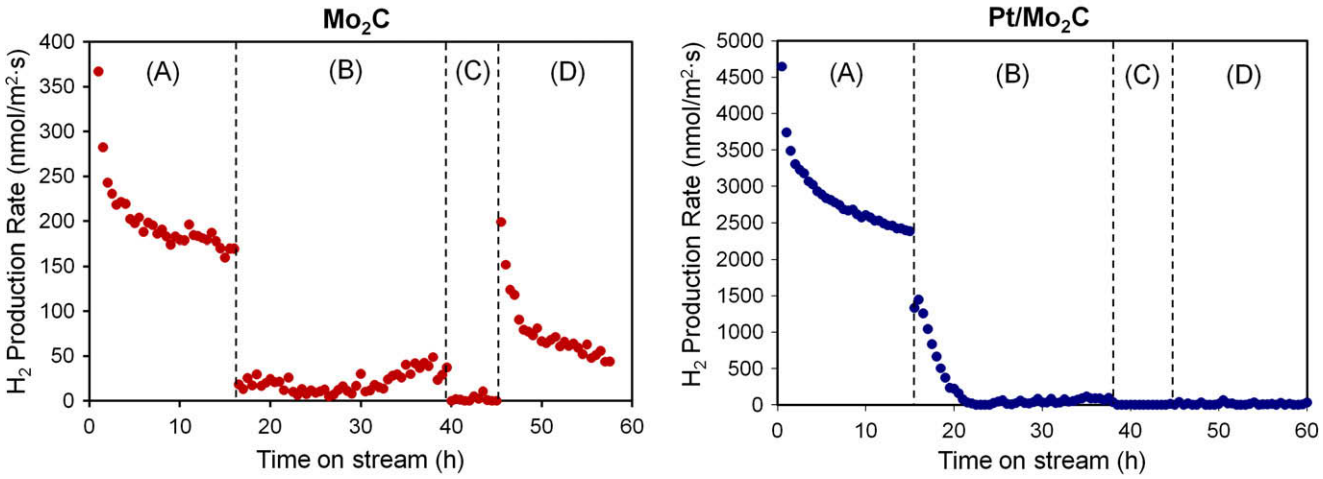

Fig. 5. Hydrogen production rates for the Mo_2C and Pt/Mo_2C catalysts with (A) sulfur-free reformate, (B) reformate with 5 ppm H_2S, (C) sulfur-free reformate, and (D) sulfur-free reformate after treatment of the catalyst at 590 °C for 4 h in a mixture of 15% CH_4/H_2. The reformate contained 9% CO, 30% H_2O, 6% CO_2, 39% H_2, and 16% N_2.

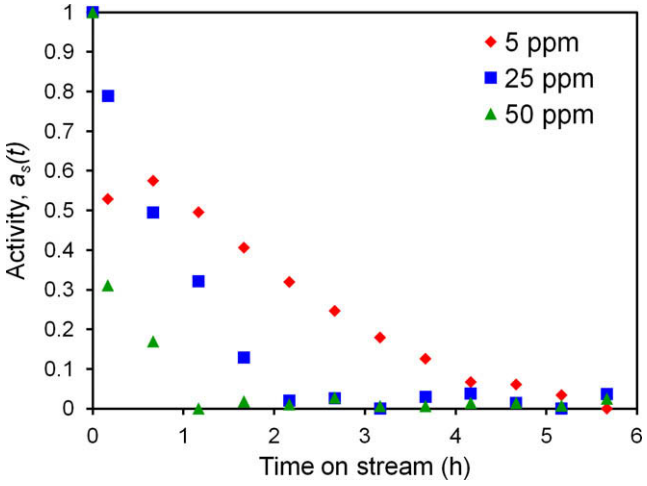

Fig. 6. Activity, $a_s(t)$, for the Pt/Mo_2C catalyst as a function of time on stream after the introduction of 5, 25, and 50 ppm H_2S to the reformate.

3.3. In situ characterization

Prior to collection of the *in situ* XPS spectra, the materials were pretreated in 15% CH_4/H_2 at 590 °C for 4 h, exposed to a reformate containing 9% CO, 30% H_2O, 6% CO_2, 39% H_2 in N_2 at 240 °C for 4 h, purged with N_2, then cooled to room temperature in the XPS reaction chamber. After reducing the pressure to $<10^{-8}$ Torr, the material was transferred into the analysis chamber. Compared to the pretreated material, the C 1s spectrum (Fig. 7) for the Mo_2C catalyst presented peaks associated with C-O and C═O, in addition to a prominent carbidic carbon peak. The resulting Mo spectra for this catalyst were similar to that for the pretreated catalyst; however, the oxygen spectra were different. In addition to peaks at 530.7 ± 0.2 and 532.4 ± 0.2 eV (also observed for the pretreated materials), a peak at 533.7 ± 0.2 eV was observed (Table 7). This peak is believed to correspond to oxygen in adsorbed carbon oxides [24]. Under reaction conditions, the O/Mo ratio for the Mo_2C catalyst was 5.7, compared to a O/Mo ratio of 1.5 for the pretreated material. This increase in the O/Mo ratio was due to an increase in the density of adsorbed O^-, OH^-, and/or H_2O, and not to an increase in Mo oxides.

For the Pt/Mo_2C catalyst, the C and Mo spectra (Fig. 7) resembled those after pretreatment, except for an additional C 1s peak that was attributed to C═O. As observed for the Mo_2C catalyst, the oxygen spectra included an additional peak at 533.7 ± 0.2 eV that was attributed to adsorbed carbon oxides. The O/Mo ratio for the Pt/Mo_2C catalyst increased to 4.2 under reaction conditions from a value of 1.2 after pretreatment. This increase was primarily due to increases in the concentrations of O^-, OH^-, and/or H_2O.

Temporal changes in the catalyst weight during exposure to H_2S provided insight regarding the nature of interactions between the catalysts and sulfur. Prior to these measurements, the catalysts were pretreated at 590 °C for 4 h in the CH_4/H_2 mixture, then degassed in He at 240 °C for 1 h. Changes in weight were assumed to be due to the adsorption onto and/or incorporation of sulfur into the catalysts. During the first 10 min at 240 °C in a 5 ppm H_2S/He mixture, there was a rapid weight gain (Fig. 8). Subsequently, the rate of weight gain decreased, but remained somewhat steady until

Table 6
Results from nonlinear regression of activity data for the Pt/Mo_2C catalyst to four empirical decay rate laws. The WGS rates were measured using reformate containing 5, 25, and 50 ppm H_2S.

Type	Linear	Exponential	Hyperbolic	Reciprocal power
Differential form	$-\frac{da_s}{dt} = k_{d,s}C^n_{H_2S,0}$	$-\frac{da_s}{dt} = k_{d,s}C^n_{H_2S,0}a_s$	$-\frac{da_s}{dt} = k_{d,s}C^n_{H_2S,0}a_s^2$	$-\frac{da_s}{dt} = k_{d,s}C^n_{H_2S,0}A_0^{1/5}a_s^m$
Integral form	$a_s = 1 - k_{d,s}C^n_{H_2S,0}t$	$a_s = e^{-k_{d,s}C^n_{H_2S,0}t}$	$a_s = \frac{1}{1+k_{d,s}C^n_{H_2S,0}t}$	$a_s = A_0 t^{-k_{d,s}C^n_{H_2S,0}}$
n	0.38 ± 0.06	0.51 ± 0.05	0.6 ± 0.1	0.1 ± 0.3
$k_{d,s}$ ($ppm^{-n}\,h^{-1}$)	0.12 ± 0.02	0.25 ± 0.03	0.5 ± 0.1	0.6 ± 0.5
A_0	–	–	–	0.31 ± 0.04
R^2_{adj}	0.781	0.986	0.965	0.737
F[a]	39.7	777	304	18.4

[a] Calculated by dividing the mean square model by the mean square error. P value for all models was <0.0001.

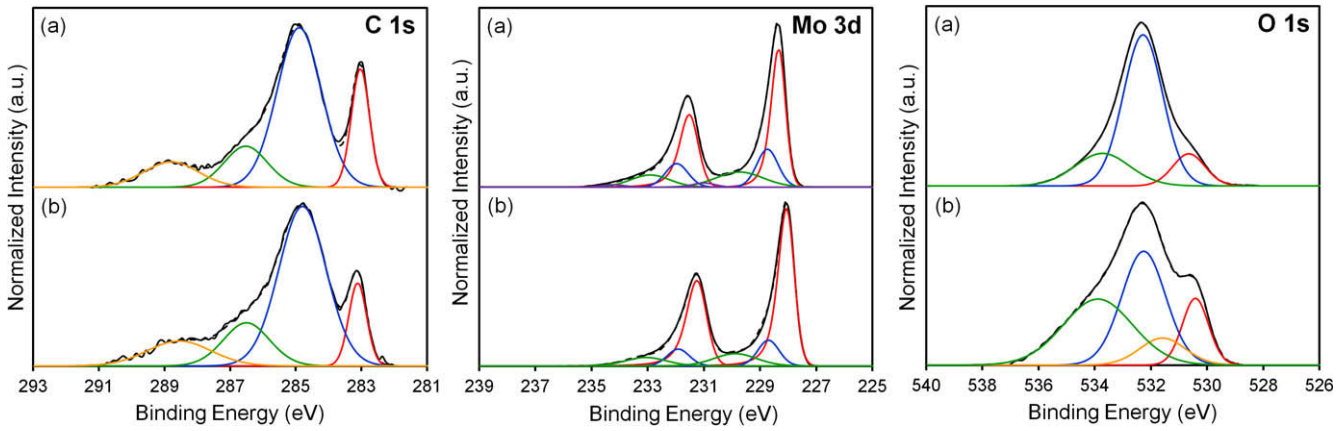

Fig. 7. C 1s, Mo 3d, and O 1s XPS spectra for the (a) Mo_2C and (b) Pt/Mo_2C catalysts following pretreatment in 15% CH_4/H_2 at 590 °C for 4 h and exposure to reformate containing 9% CO, 30% H_2O, 6% CO_2, 39% H_2, and 16% N_2 at 240 °C in the *in situ* XPS reaction chamber.

Table 7
Binding energies from *in situ* spectra for species on surfaces of the Mo_2C and Pt/Mo_2C catalysts following pretreatment in 15% CH_4/H_2 at 590 °C for 4 h, exposure to reformate containing 9% CO, 30% H_2O, 6% CO_2, 39% H_2 in N_2 at 240 °C for 4 h, purge with N_2, then cooling to room temperature.

Catalyst	C 1s (eV)[a,b]		Mo $3d_{5/2}$ (eV)[a]			Pt $4f_{7/2}$ (eV)[a]		O 1s (eV)[a]		
	Mo_2C	C—O	Mo^{2+}	$Mo^{\delta+}$	Mo^{4+}	Pt^0	Pt^{2+}	MoO_x	O^-, OH^-, H_2O, O═C	O—C
Mo_2C	283.1 (18)	286.5 (14)	228.3 (55)	228.7 (23)	229.7 (20)	–	–	530.7 (12)	532.3 (68)	533.7 (20)
Pt/Mo_2C	283.2 (11)	286.5 (16)	228.2 (69)	228.7 (16)	229.9 (15)	71.6 (83)	73.3 (17)	530.5 (14)	532.3 (40)	533.9 (36)

[a] The number in parentheses represents the atomic percentage.
[b] Balance of atomic percentages for C 1s is adventitious carbon.

reaching a weight gain equivalent to ~2 monolayers (ML) of sulfur, based on a site density of 10 sites/nm^2 and 1 sulfur atom/site. After the adsorption or incorporation of ~2 ML of sulfur, the rate of weight gain slowed then leveled off. The overall rate of sulfur uptake was slightly higher for the Pt/Mo_2C catalyst than for the Mo_2C catalyst, and shapes of the curves were different suggesting that the presence of Pt caused a change in the mechanism for sulfur incorporation.

Hydrogen sulfide readily dissociates on Mo_2C at room temperature [42], and the conversion of Mo_2C and H_2S to MoS_2 is thermodynamically favorable with a ΔG_f of −264 kJ/mol at 240 °C [43]. Furthermore, it has been reported that H_2S dissociates on Pt at temperatures as low as 100 °C [44]. The formation of PtS from Pt and H_2S is also thermodynamically favorable with a ΔG_f of −32 kJ/mol at 240 °C.

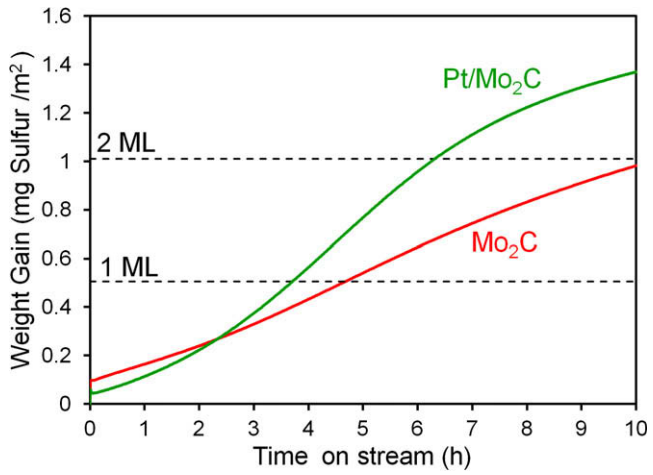

Fig. 8. Weight gain during exposure of the Mo_2C and Pt/Mo_2C catalysts to 5 ppm H_2S in He at 240 °C. The dashed lines indicate the weight gains corresponding to 1 ML and 2 ML of sulfur coverage assuming a material with 98 m^2/g.

3.4. Post-reaction ex situ characterization

Bulk crystalline structures for the Mo_2C and Pt/Mo_2C catalysts did not change on exposure to reformate without or with 5 ppm

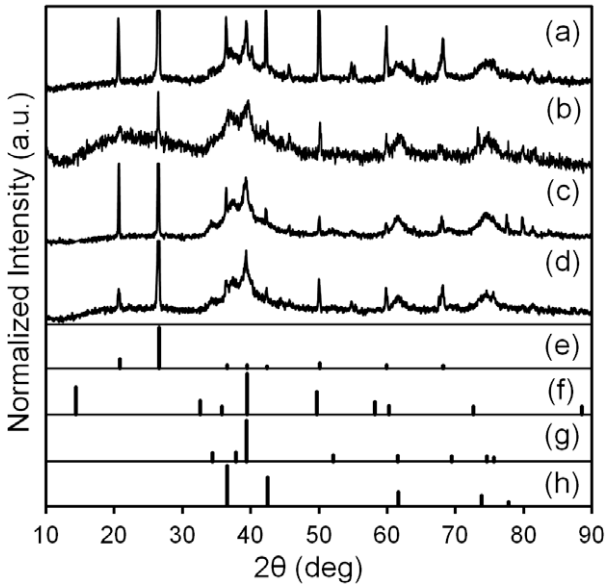

Fig. 9. X-ray diffraction patterns for the (a) Mo_2C catalyst after WGS without H_2S, (b) Pt/Mo_2C catalyst after WGS without H_2S, (c) Mo_2C catalyst after WGS with 5 ppm H_2S, and (d) Pt/Mo_2C catalyst after WGS with 5 ppm H_2S. Peak positions for polycrystalline (e) SiO_2 [45], (f) MoS_2 [46], (g) β-Mo_2C [20], and (h) α-MoC_{1-x} [21] reference materials are also illustrated. The SiO_2 was used as a catalyst diluent during the reaction rate measurements.

H_2S at 240 °C, as evident from the XRD patterns (Fig. 9). The sharper peaks were due to the SiO_2 that was used as a diluent during the reaction rate measurements. The absence of a peak at $2\theta \sim 14°$ indicated that MoS_2 crystallites, if present, were below the detection limit of the X-ray diffractometer. Micrographs of the fresh and spent catalysts (see for example Fig. 10) were very similar, indicating that there were no significant changes in the surface morphology. Although thermodynamically favorable, Mo_2C and Pt are reported to be moderately resistant to bulk sulfidation, possibly because the diffusion of sulfur into the sub-surface is slow due to its size [2,43,47,48]. Surface areas for the spent catalysts both in sulfur-free and in sulfur-containing reactants were ~5–15% lower than those for the fresh catalysts. For example, surface areas for the spent Mo_2C catalysts were 86 ± 4 (without sulfur) and 93 ± 4 m^2/g (with sulfur) compared to a surface area of 98 ± 5 m^2/g for the as-synthesized catalyst. These results confirm that the deactivation caused by exposure to H_2S was not due to surface area loss or sintering.

Due to the difficulty of ensuring the complete removal of sulfur, experiments involving sulfur could not be carried out in the XPS reaction system. Instead, catalysts exposed to reformate in the catalytic reactor were cooled to room temperature, quickly transferred in air to a desiccator, and stored under vacuum until being transferred to the spectrometer and collection of the *ex situ* spectra. A comparison of the *in situ* (Fig. 7) and *ex situ* (Fig. 11) Mo spectra for materials exposed to the reformate suggests that this brief exposure to air caused partial oxidation of Mo_2C at the surface to MoO_3. As shown in Fig. 9, however, the catalysts did not undergo bulk oxidation to MoO_2 or MoO_3 upon exposure to air. Nevertheless, an examination of major changes in the *ex situ* spectra provided insight regarding the significant effects of sulfur on the Mo_2C and Pt/Mo_2C catalysts. Results from deconvolution of the *ex situ* spectra are summarized in Table 8 for catalysts subjected to the following treatments (also see Fig. 5):

(A) sulfur-free reformate at 240 °C for 16 h;
(B) reformate with 5 ppm H_2S at 240 °C for 22 h;
(C) sulfur-free reformate at 240 °C for 5 h;
(D) sulfur-free reformate after treatment of the catalyst at 590 °C in CH_4/H_2 for 4 h.

With the exception of the S 2p spectra, spectra for the Mo_2C catalyst prior to and after exposure to sulfur were similar. Exposure to reformate with 5 ppm H_2S resulted in a doublet with a S $2p_{3/2}$ peak at

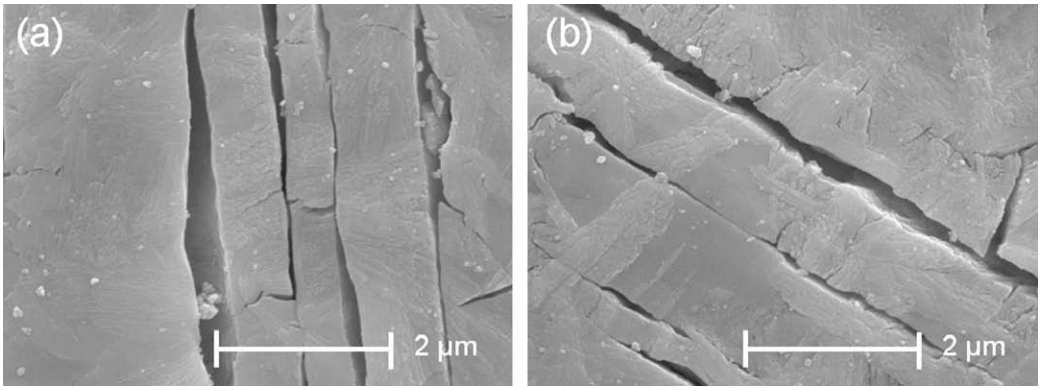

Fig. 10. Scanning electron micrographs of the (a) as-synthesized and (b) spent (WGS with 5 ppm H_2S at 240 °C) Mo_2C catalysts. Images were collected at 15 kV accelerating voltage, 3.0 spot size, and 18,000 magnification.

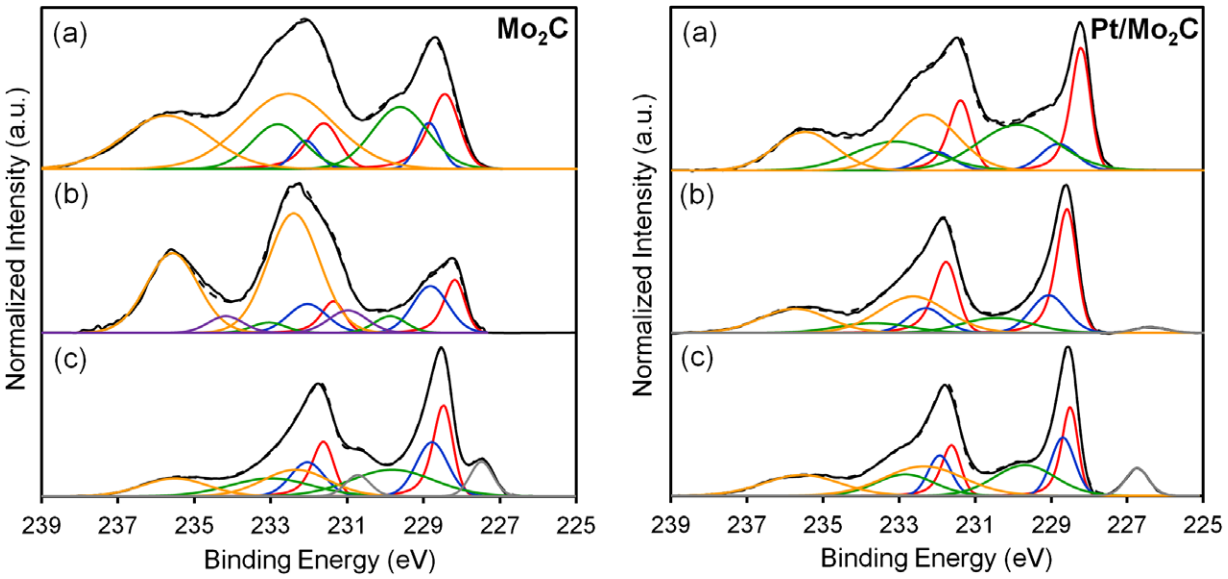

Fig. 11. Mo 3d XPS spectra for the Mo_2C and Pt/Mo_2C catalysts (a) after WGS without H_2S, (b) after WGS with 5 ppm H_2S, and (c) after WGS with 5 ppm H_2S, treatment in 15% CH_4/H_2 at 590 °C for 4 h, and WGS without H_2S.

Table 8
Binding energies from *ex situ* spectra for species on the surfaces of the Mo_2C and Pt/Mo_2C catalysts following measurement of the reaction rates (see Fig. 5).

Catalyst	Treatment[a]	C 1s (eV)[b,c]		Mo $3d_{5/2}$ (eV)[b]			Pt $4f_{7/2}$ (eV)[b]			O 1s (eV)[b]			S 2p (eV)[b]					S 2s (eV)[b]
		Mo_2C	C—O	Mo^{2+}	$Mo^{\delta+}$	Mo^{4+}	Mo^{6+}	Pt*	Pt^0	Pt^{2+}	MoO_x	O⁻, OH^-, H_2O, O=C	O–C	MoS_xC_y	S–Mo	MoS_2/PtS	S_2^{2-}	SO_2^{4-}	
Mo_2C	A	283.3 (10)	286.6 (35)	228.4 (15)	228.8 (8)	229.6 (26)	232.5 (51)	–	–	–	530.6 (30)	532.6 (39)	533.8 (31)	–	–	–	–	–	–
Mo_2C	ABC	–	285.8 (36)	228.2 (10)	228.8 (16)	229.9 (5)	232.4 (60)	–	–	–	530.6 (9)	532.8 (80)	533.7 (11)	–	–	–	163.1 (100)	–	–
Mo_2C	ABCD	283.6 (27)	286.3 (22)	228.5 (21)	228.8 (21)	229.8 (27)	232.3 (21)	–	–	–	530.7 (62)	532.4 (30)	533.5 (8)	160.7 (18)	161.7 (37)	162.3 (45)	–	–	–
Pt/Mo_2C	A	283.1 (35)	286.7 (7)	228.2 (22)	228.8 (9)	229.9 (35)	232.3 (34)	69.7 (26)	71.5 (71)	73.3 (3)	530.6 (64)	532.2 (29)	533.8 (3)	–	–	–	–	–	–
Pt/Mo_2C	ABC	283.6 (22)	286.4 (22)	228.6 (33)	229.0 (19)	230.4 (14)	232.6 (34)	–	71.9 (71)	72.7 (29)	530.8 (55)	532.1 (31)	533.7 (2)	–	161.9 (23)	162.5 (59)	–	168.8 (18)	226.4
Pt/Mo_2C	ABCD	283.6	286.4	228.5	228.7	229.7	232.4	70.5	72.0	73.4	530.8	532.1 (43)	533.6	160.3	161.9	162.4	–	168.9	226.7
		(17)	(20)	(19)	(20)	(27)	(34)	(24)	(73)	(3)	(49)		(2)	(11)	(14)	(58)		(17)	

[a] Treatments correspond to sections of Fig. 5.
[b] The number in parentheses represents the atomic percentage.
[c] Balance of atomic percentages for C 1s is adventitious carbon.

163.1 ± 0.2 eV (Fig. 12). This binding energy is consistent with the presence of S_2^{2-} in MoS_3 or SH groups [2,49].

Treatment of the sulfur-deactivated Mo_2C catalyst in 15% CH_4/H_2 at 590 °C for 4 h caused an increase in the relative amounts of Mo that we attributed to Mo_2C and MoS_2 [2,32] (Fig. 11) and emergence of a small doublet with Mo $3d_{5/2}$ peak at 227.5 ± 0.1 eV. This doublet is consistent with the presence of Mo^0 [50]. Three doublets were resolved in the S 2p spectra (Fig. 12). The doublet with S $2p_{3/2}$ peak at 161.8 ± 0.1 eV has been assigned to atomic sulfur strongly adsorbed to Mo [51,52]. The peak at 162.4 ± 0.1 eV corresponds to S^{2-} species, likely in the form of MoS_2 [2,29,48]. The peak at 160.5 ± 0.2 eV has been tentatively attributed to a Mo sulfidocarbide [47,53,54] based on the position.

Exposure of the Pt/Mo_2C catalyst to sulfur significantly affected the associated XPS spectra. Spectra following exposure to sulfur-free reformate contained a doublet with Pt $4f_{7/2}$ peak at 70.1 ± 0.4 eV (Fig. 13), in addition to peaks attributable to Pt^0 and PtO. This binding energy does not match those of any previously reported Pt species, but the shift relative to Pt^0 is consistent with the presence of anionic Pt. Exposure to sulfur eliminated this highly reduced Pt species. The relative amount of Mo_2C increased following exposure to reformate containing 5 ppm H_2S. Three doublets were resolved in the S 2p spectra for the Pt/Mo_2C catalyst after exposure to reformate with 5 ppm H_2S at 240 °C (Fig. 12). The doublet with S $2p_{3/2}$ peak at 161.8 ± 0.1 eV corresponds to sulfur strongly adsorbed to Mo. The doublet with S $2p_{3/2}$ peak at 162.4 ± 0.1 eV corresponds to S^{2-} species, possibly in the form of MoS_2 or PtS [2,29,48,55,56]. The doublet with S $2p_{3/2}$ peak at 168.8 ± 0.1 eV is consistent with the presence of sulfate species (S^{6+}) [32,57,58]. Oxygen in the sulfate might have been introduced from the sub-surface or exposure to air. Treatment of the sulfur-deactivated Pt/Mo_2C catalyst in 15% CH_4/H_2 at 590 °C for 4 h caused reemergence of peaks that we attributed to anionic Pt and Mo sulfidocarbide, a slight decrease in the amount of Mo_2C and slight increase in the amount of MoS_2.

4. Discussion

Sulfur tolerance can be manifested in two ways. The most attractive form of tolerance is when the catalyst maintains its rate during exposure to sulfur. Another form is when the catalytic activity can be restored via modest treatment of the spent material. Results described in this paper indicate that the Mo_2C and Pt/Mo_2C catalysts possessed some degree of sulfur tolerance. The Mo_2C catalyst was significantly deactivated during exposure to sulfur but maintained a modest rate, and some of the initial performance could be restored via treatment in CH_4/H_2 mixtures. The Pt/Mo_2C catalyst behaved in a similar manner with the exception that the extent of reactivation was much lower than that for the Mo_2C catalyst. This discussion section will explore changes in the surface chemistry that correlate with deactivation of these catalysts.

The Mo_2C and Pt/Mo_2C catalysts deactivated during the first 10–15 h of exposure to sulfur-free reformate (Fig. 5). Rate decay equations suggested that the deactivation was caused by carbon deposition. This result is in agreement with XPS findings. Comparison of XPS spectra from pretreated and in-situ WGS exposed samples revealed an increase in carbon oxide groups (C—O and C=O) as well as surface oxygen. Formation of carbonate or formate groups may have caused blockage of active sites as has been reported for Au/CeO_2 catalysts [59]. Formation of surface oxides could reduce the number of active Mo_2C sites. This deactivation mechanism will be the subject of a future paper.

Deactivation of the Mo_2C catalyst by H_2S appeared to occur in three stages. The reaction rate decreased significantly during the first 10 min of exposure to sulfur. In a similar time frame, the sulfur

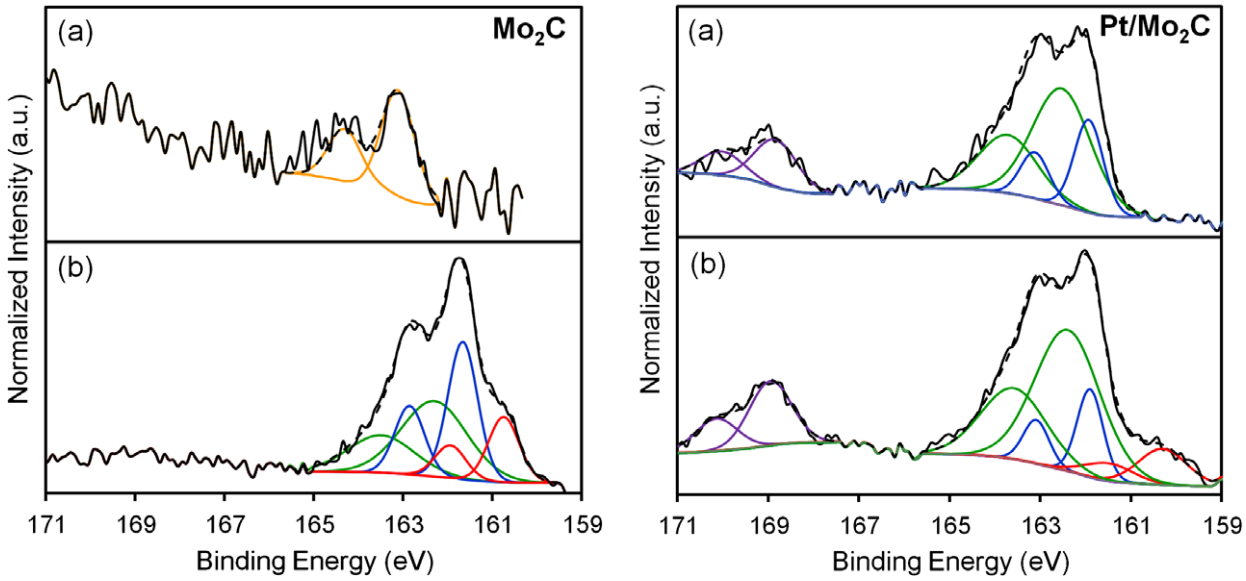

Fig. 12. S 2p XPS spectra for the Mo_2C and Pt/Mo_2C catalysts (a) after WGS with 5 ppm H_2S for 22 h and (b) after WGS with 5 ppm H_2S, treatment in 15% CH_4/H_2 at 590 °C for 4 h, and WGS without H_2S.

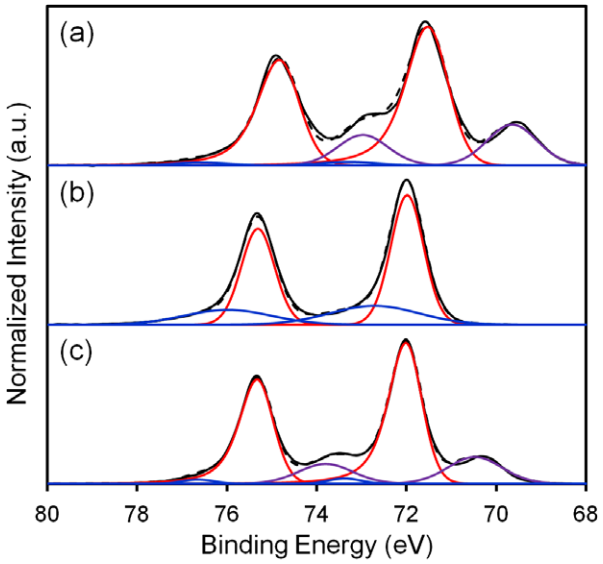

Fig. 13. Pt 4f XPS spectra for the Pt/Mo_2C catalyst (a) after WGS without H_2S, (b) after WGS with 5 ppm H_2S, and (c) after WGS with 5 ppm H_2S, treatment in 15% CH_4/H_2 at 590 °C for 4 h, and WGS without H_2S.

adsorption and/or incorporation rate increased dramatically. We believe these responses were interrelated and that highly active Mo_2C sites were quickly poisoned during this stage. Subsequently, the WGS rate decreased and the sulfur content increased more gradually. During the final stage, the activity increased slightly. This increase in activity appeared to correspond with the adsorption and/or incorporation of ~2 ML of sulfur on the Mo_2C catalyst surface. When sulfur was removed from the reactant, the activity decreased suggesting that it was associated with MoS_2 nanoparticles. Molybdenum sulfide is known to be active for the WGS in the presence of H_2S, and in fact, requires sulfur in the feed to maintain its activity [60]. A fraction of the Mo_2C sites could be restored via treatment in 15% CH_4/H_2 at 590 °C for 4 h; however, based on the XPS results, MoS_2 sites persisted. Therefore, we have concluded that the sulfur tolerance exhibited by the Mo_2C catalyst was associated with MoS_2 nanoparticles produced via sulfidation of Mo_2C, and the regenerability of highly active Mo_2C-based sites poisoned during initial exposure to sulfur.

In comparison to the Mo_2C catalyst, the Pt/Mo_2C catalyst exhibited a much slower deactivation rate, suggesting that most of the activity was associated with the presence of Pt. The results are consistent with two types of sites on the Pt/Mo_2C catalyst: sites on the Pt nanoparticles or at the Pt nanoparticle–Mo_2C support interface, and sites on the Mo_2C support. The high activity Pt-based sites were severely and irreversibly deactivated, we believe, as a consequence of the conversion of Pt into inactive PtS. Sites associated with the Mo_2C support could be partially reactivated in a manner similar to that observed for the Mo_2C catalyst.

Finally, we note that surface oxygen may have played a role in the interactions of sulfur with the Mo_2C and Pt/Mo_2C catalysts. Oxygen has been reported to facilitate the sulfidation of early transition metal carbides and nitrides [29]. The O/Mo ratios for the Mo_2C and Pt/Mo_2C catalysts were very high and each contained substantial amounts of MoS_2 after WGS in the presence of H_2S. The increased O/Mo ratio after exposure to WGS reactants was primarily associated with the presence of strongly adsorbed O^-, OH^-, O═C, and/or H_2O. This oxygen may have facilitated the formation of MoS_2. Future experiments will explore this behavior.

5. Conclusions

The effects of H_2S on the WGS activities, structures, and compositions of Mo_2C and Pt/Mo_2C catalysts have been investigated. These catalysts were severely deactivated on exposure to H_2S but could be partially regenerated. Characterization of the spent catalysts suggested that deactivation of the Mo_2C catalyst was primarily due to the adsorption of sulfur on Mo_2C sites and the formation of surface MoS_2. The MoS_2 sites were active in the presence of sulfur. Deactivation of the Pt/Mo_2C catalyst appeared to be primarily due to the irreversible sulfidation of Pt nanoparticles. Other features for this catalyst were similar to those for the Mo_2C catalyst. Under reaction conditions, the Mo_2C and Pt/Mo_2C surfaces also possessed high concentrations of oxygen, which may have facilitated formation of the Mo sulfide. Although Pt improved the activity of the Mo_2C catalyst, it also altered the interaction of sulfur with the catalyst surface, resulting in an increased susceptibility to

sulfur poisoning. These results suggest that the Mo_2C and Pt/Mo_2C catalysts were partially tolerant to sulfur during WGS.

Acknowledgments

This work was supported by funding from the Department of Energy, the National Science Foundation, and the Hydrogen Energy Technology Laboratory at the University of Michigan.

References

[1] J.M. Robinson, S.R. Barrett, K. Nhoy, R.K. Pandey, J. Phillips, O.M. Ramirez, R.I. Rodriguez, Energy Fuels 23 (2009) 2235.
[2] P.K. Cheekatamarla, W.J. Thomson, Appl. Catal. A 287 (2005) 176.
[3] P. Da Costa, J.-L. Lemberton, C. Potvin, J.-M. Manoli, G. Perot, M. Breysse, D. Djega-Mariadassou, Catal. Today 65 (2001) 195.
[4] P.A. Aegerter, W.W.C. Quigley, G.J. Simpson, D.D. Ziegler, J.W. Logan, K.R. McCrea, S. Glazier, M.E. Bussell, J. Catal. 164 (1996) 109.
[5] M.K. Neylon, S.K. Bej, C.A. Bennett, L.T. Thompson, Appl. Catal. A 232 (2002) 13.
[6] F.H. Ribeiro, R.A.D. Betta, M. Boudart, J. Baumgartner, E. Iglesia, J. Catal. 130 (1991) 86.
[7] J.S. Lee, S. Locatelli, S.T. Oyama, M. Boudart, J. Catal. 125 (1990) 157.
[8] G.S. Ranhotra, A.T. Bell, J.A. Reimer, J. Catal. 108 (1987) 40.
[9] M.B. Zellner, J.G. Chen, Catal. Today 99 (2005) 299.
[10] R. Venkataraman, H.R. Kunz, J.M. Fenton, J. Electrochem. Soc. 150 (2003) 278.
[11] H. Zhong, H. Zhang, G. Liu, Y. Liang, J. Hu, B. Yi, Electrochem. Commun. 8 (2006) 707.
[12] L.T. Thompson, S.K. Bej, J.J. Patt, C.H. Kim, US Patent 6897178 (2005).
[13] T.E. King, Ph.D. Thesis, University of Michigan, 2007.
[14] W. Setthapun, S. Bej, L.T. Thompson, Top. Catal. 49 (2008) 73.
[15] Q. Ming, T. Healey, L. Allen, P. Irving, Catal. Today 77 (2002) 51.
[16] Satterfield, Heterogeneous Catalysis in Industrial Practice, Second ed., McGraw-Hill, 1991. p. 445.
[17] Y.-M. Wu, Oil Gas J. 92 (1994) 38.
[18] J. Patt, Ph.D. Thesis, University of Michigan, 2003.
[19] J. Patt, D.J. Moon, C. Phillips, L. Thompson, Catal. Lett. 65 (2000) 193.
[20] S. Nagakura, M. Kikuchi, S. Oketani, Acta Crystallogr. 21 (1966) 1009.
[21] J.C. Schuster, H. Nowotny, Monatsh. Chem. 110 (1979) 321.
[22] M. Ghedira, C. Do-Dinh, M. Marezio, J. Mercier, J. Solid State Chem. 59 (1985) 159.
[23] J.D. Hanawalt, H.W. Rinn, L.K. Frevel, Anal. Chem. 10 (1938) 457.
[24] C.A. Vanderborgh, Y.K. Vohra, H. Xia, A.L. Ruoff, Phys. Rev. B: Condens. Matter Mater. Phys. 41 (1990) 7338.
[25] H. Iida, A. Igarashi, Appl. Catal. A 298 (2006) 152–160.
[26] T.P. St. Clair, S.T. Oyama, D.F. Cox, S. Otani, Y. Ishizawa, R.-L. Lo, K.-I. Fukui, Y. Iwasawa, Surf. Sci. 426 (1999) 187.
[27] P. Delporte, F. Meunier, C. Pham-Huu, P. Vennegues, M.J. Ledoux, J. Guille, Catal. Today 23 (1995) 251.
[28] M. Buo, J.M. Martin, T. Le Mogne, L. Vovelle, Appl. Surf. Sci. 47 (1991) 149.
[29] Z.B. Zhaobin Wei, P. Grange, B. Delmon, Appl. Surf. Sci. 135 (1998) 107.
[30] J.-G. Choi, L.T. Thompson, Appl. Surf. Sci. 93 (1996) 143.
[31] A. Katrib, P. Leflaive, L. Hilaire, G. Maire, Catal. Lett. 38 (1996) 95.
[32] A.S. Mamede, J.-M. Giraudon, A. Lofberg, L. Leclercq, G. Leclercq, Appl. Catal. A 227 (2002) 73.
[33] M.J. Ledoux, C.P. Huu, J. Guille, H. Dunlop, J. Catal. 134 (1992) 383.
[34] P. Perez-Romo, C. Potvin, J.-M. Manoli, M.M. Chehimi, G. Djega-Mariadassou, J. Catal. 208 (2002) 187.
[35] J.L.G. Fierro, J.M. Palacios, F. Tomas, Surf. Interface Anal. 13 (1988) 25.
[36] J.P. Contour, G. Mouvier, M. Hoogewys, C. Leclere, J. Catal. 48 (1977) 217.
[37] G.M. Bancroft, I. Adams, L.L. Coatsworth, C.D. Bennewitz, J.D. Brown, W.D. Westwood, Anal. Chem. 47 (1975) 586.
[38] H.S. Fogler, Elements of Chemical Reaction Engineering, third ed., Prentice Hall, New Jersey, 1999. p. 643.
[39] A. Voorhies Jr., Ind. Eng. Chem. 37 (1945) 318.
[40] C.G. Rudershausen, C.C. Watson, Chem. Eng. Sci. 3 (1954) 110.
[41] C.H. Bartholomew, R.J. Farrauto, Fundamentals of Industrial Catalytic Processes, second ed., John Wiley and Sons, Berlin, 2006.
[42] J.A. Rodriguez, J. Dvorak, T. Jirsak, J. Phys. Chem. B 104 (2000) 11515.
[43] E. Furimsky, Appl. Catal. A 240 (2003) 1.
[44] M.V. Mathieu, M. Primet, Appl. Catal. 9 (1984) 361.
[45] V.I. Pakhomov, A.V. Goryunov, P.V. Pakhomov, N.T. Chibiskova, Zh. Neorg. Khim. 38 (1993) 44.
[46] V. Petkov, S.J.L. Billinge, P. Larson, S.D. Mahanti, T. Vogt, K.K. Rangan, M.G. Kanatzidis, Phys. Rev. B: Condens. Matter Mater. Phys. 65 (2002) 1.
[47] E.J. Markel, J.W. Van Zee, J. Catal. 126 (1990) 643.
[48] Z. Paal, P. Tetenyi, M. Muhler, U. Wild, J.-M. Manoli, C. Potvin, J. Chem. Soc., Faraday Trans. 94 (1998) 459.
[49] Th. Weber, J.C. Muijsers, J.W. Niemantsverdriet, J. Phys. Chem. 99 (1995) 9194.
[50] J.E. De Vries, H.C. Yao, R.J. Baird, H.S. Gandhi, J. Catal. 84 (1983) 8.
[51] J.T. Roberts, C.M. Friend, Surf. Sci. 202 (1988) 405.
[52] J.A. Rodriguez, S.Y. Li, J. Hrbek, H.H. Huang, G.-Q. Xu, J. Phys. Chem. 100 (1996) 14476.
[53] P. Liu, J.A. Rodriguez, J.T. Muckerman, J. Mol. Catal. A: Chem. 239 (2005) 116.
[54] S.P. Kelty, G. Berhault, R.R. Chianelli, Appl. Catal. A 322 (2007) 9.
[55] M. Muhler, Z. Paal, Surf. Sci. Spectra 4 (1997) 125.
[56] J. Dembowski, L. Marosi, M. Essig, Surf. Sci. Spectra 2 (1993) 104.
[57] M.-D. Appay, J.-M. Manoli, C. Potvin, M. Muhler, U. Wild, O. Pozdnyakova, Z. Paal, J. Catal. 222 (2004) 419.
[58] B.J. Lindberg, K. Hamrin, G. Johansson, U. Gelius, A. Fahlman, C. Nordling, K. Siegbahn, Phys. Scripta 1 (1970) 286.
[59] C.H. Kim, L.T. Thompson, J. Catal. 230 (2005) 66.
[60] P. Hou, D. Meeker, H. Wise, J. Catal. 80 (1983) 280.